# Disturbances in Pipe Flow Excited by Magnetic Fields

U. Brosa

Fachbereich Physik der Philipps-Universität Marburg and Brosa GmbH, Amöneburg, Germany

Z. Naturforsch. **46a**, 473–480 (1991); received February 22, 1991

Defined disturbances of laminar flow in a pipe can be excited by magnetic fields. This is important for investigations concerning the onset of turbulence in a pipe. A theory of these disturbances is derived and thus a criterion established to discriminate the induction of the so-called mothers from the excitation of daughters. The conditions to optimize the effects and the inferences for the experimental setup are discussed.

PACS number: 47.25.Ac

## 1. What's the Use of Defined Disturbances?

A substantial breakthrough in hydrodynamic research was the verification of Tollmien-Schlichting waves [1] by Schubauer and Skramstad [2]. It was that important because it revealed a doorway to turbulence in boundary layers. As soon as such a doorway is known, means to control turbulence can be considered. For boundary layers, the Tollmien-Schlichting theory has led meanwhile to applications in aircraft construction [3], namely to the so-called laminar profiles of wings.

The fundamental idea of Schubauer and Skramstad was to excite defined disturbances, with known amplitude and wavelength. This was in marked contrast to many other approaches where turbulence was induced randomly. Schubauer and Skramstad installed a ribbon over the wall confining the boundary layer and forced it to vibrate. We will call this kind of approach the mechanical method.

Even though it is presented in very many textbooks as *the* example of turbulence, flow in a pipe is much less understood than boundary-layer flow. Firstly this is so because the translation of the Tollmien-Schlichting theory to the cylindrical geometry doesn't give positive results: Obviously there is no transition of pipe flow to turbulence which can be described by a linear eigenvalue theory. Secondly, it is more difficult to excite a defined disturbance in a pipe, simply because of the cylindrical geometry. The most fruitful endeavors I'm aware of were those by Leite [4]. He inserted obstacles of different shapes into pipes and observed the resulting disturbances. However, these experiments did not yield conclusive results since the obstacles primarily created complicated eddies. Wavelength and strength of the resulting disturbances could not be controlled directly. Another drawback was the fixed mounting of the obstacles. Time-dependent features developed only because of eddy detachment.

Meanwhile there seems to be progress with the pipe. Simulations of the nonlinear Navier-Stokes equation and a theory of the essentials has shown that the cause of the transition can be unveiled by a linear theory which takes into account not only the eigenvalues but also the eigenvectors [5]. The theory predicts a certain class of disturbances as doorways to turbulence. Experimental verifications are under way [6]. One approach is via the mechanical method: Parts of the solid pipe wall are replaced by elastic materials which can be deformed into virtually arbitrary shapes [7]. Another approach is to create an electrical current through the pipe, in addition to the hydrodynamic flow. With suitable magnets the flow can be deflected and a great variety of disturbances induced [8]. This is what we call the magnetic method. Both methods can act gently such as to produce no eddies but only sinusoidal deflections, and their time dependence can be imposed at will.

Here a linear theory of the magnetic method will be presented. In Sect. 2, the fundamental equations of motion will be simplified to leave only the features absolutely necessary. Only two parameters remain: the Reynolds and Mach-Alfvén numbers. Since at the onset disturbances are small, a linear description may be permitted. In Sect. 3, the electromagnetic part of the problem will be solved, and two classes of magnetic fields will be discussed: the flat and the curved

Reprint requests to Dr. U. Brosa, Fachbereich Physik, Universität Marburg and Brosa GmbH, Am Brücker Tor 4, W-3572 Amöneburg, FRG.

0932-0784 / 91 / 0600-0473 $ 01.30/0. – Please order a reprint rather than making your own copy.

fields. It will turn out that they are suited differently for the induction of turbulence. This will be shown in Sect. 4, with the solution of the equations of motion.

## 2. Posing the Problem and Boiling it Down

Fundamental is the Navier-Stokes equation

$$\varrho_0 \frac{\mathrm{d}\boldsymbol{U}}{\mathrm{d}t} = -\nabla P - \eta_0 \nabla \times \nabla \times \boldsymbol{U} + \boldsymbol{J} \times \boldsymbol{B} \quad \text{with} \quad \nabla \cdot \boldsymbol{U} = 0 \tag{1}$$

for an incompressible fluid with constant density $\varrho_0$ and viscosity $\eta_0$. Pressure $P(\boldsymbol{r}, t)$ and velocity $\boldsymbol{U}(\boldsymbol{r}, t)$ depend on space $\boldsymbol{r}$ and time $t$. The velocity is coupled to the electromagnetic fields via the Lorentz force $\boldsymbol{J} \times \boldsymbol{B}$ containing electric current $\boldsymbol{J}(\boldsymbol{r}, t)$ and magnetic field $\boldsymbol{B}(\boldsymbol{r}, t)$. Generally, the electromagnetic fields have dynamics on their own as described by Maxwell's equations

$$\nabla \times \boldsymbol{B} = \mu_0 \boldsymbol{J}, \qquad \nabla \cdot \boldsymbol{B} = 0, \tag{2}$$

$$\nabla \times \boldsymbol{E} = -\frac{\partial \boldsymbol{B}}{\partial t}, \qquad \nabla \cdot \boldsymbol{E} = 0, \tag{3}$$

with the constant magnetic permeability $\mu_0$. Electric charge and displacement current are entirely unimportant in hydromagnetic problems [9]. The system needs to be closed by Ohm's law

$$\boldsymbol{J} = \sigma_0 (\boldsymbol{E} + \boldsymbol{U} \times \boldsymbol{B}) . \tag{4}$$

$\sigma_0$ signifies a constant conductivity.

It shall be shown that the last three equations can be reduced to

$$\nabla \times \boldsymbol{B} = 0, \quad \nabla \cdot \boldsymbol{B} = 0, \tag{5}$$

$$\nabla \times \boldsymbol{E} = 0, \quad \nabla \cdot \boldsymbol{E} = 0 \tag{6}$$

and

$$\boldsymbol{J} = \sigma_0 \boldsymbol{E}, \tag{7}$$

meaning that there is no feedback of the fluid to the electromagnetic fields. Such simplifications are admissible only if the relevant parameters take certain orders of magnitude. See Table 1 for a list.

To justify the neglect of Ørsted's term in (5), it should be appreciated that the magnetic field $B$ created by the electric current $J_0$ is much smaller than $B_0$ generated by the external magnets. By an order-of-magnitude estimation we find $B = R_0 \mu_0 J_0$. According to Table 1 this is $10^{-4}\ \mathrm{V\,m^2\,s}$, four powers of ten smaller than $B_0$.

Table 1. Constants and parameters relevant for the magnetic excitation of disturbances in pipe flow. Only orders of magnitude matter. The units are kilogram, meter, second, Volt, Ampère.

| Quantity | Symbol | Typical value | Explanation |
|---|---|---|---|
| Length | $R_0$ | $10^{-2}\,\mathrm{m}$ | Pipe radius |
| Velocity | $U_0$ | $10^{-1}\,\mathrm{m\,s^{-1}}$ | $Re \approx 1000$ |
| Time | $t_0$ | $10^{-1}\,\mathrm{s}$ | $R_0/U_0$ |
| Fluid density | $\varrho_0$ | $10^{3}\,\mathrm{kg\,m^{-3}}$ | Water |
| Viscosity | $\nu_0$ | $10^{-6}\,\mathrm{m^2\,s^{-1}}$ | $\eta_0/\varrho_0$, water |
| Conductivity | $\sigma_0$ | $10^{2}\,\mathrm{A\,V^{-1}\,m^{-1}}$ | Salted water |
| Current density | $J_0$ | $10^{4}\,\mathrm{A\,m^{-2}}$ | |
| Electric field | $E_0$ | $10^{2}\,\mathrm{V\,m^{-1}}$ | $J_0/\sigma_0$ |
| Permeability | $\mu_0$ | $4\pi \cdot 10^{-7}\,\mathrm{V\,s\,A^{-1}\,m^{-1}}$ | Vacuum |
| Magnetic field | $B_0$ | $1\,\mathrm{V\,m^{-2}\,s}$ | one Tesla |

Likewise, why can we neglect in (6) the electric field $E$ induced by changes of the magnetic field $B_0$, i.e. Faraday's term? Again, by order of magnitude we have $E = R_0 B_0 / t_0$, which takes the value $10^{-2}\,\mathrm{V\,m^{-1}}$. Compared to $E_0$ in Table 1 this is four powers of ten too small.

Finally, to demonstrate the insignificance of the Lorentz term in Ohm's law (7), we compute $E = U_0 B_0$ and see that this is three powers of ten smaller that $E_0$.

Now let us nondimensionalize the equations of motion. We distinguish the nondimensional quantities by asterisks and insert expressions like these

$$\boldsymbol{U} = U_0 \boldsymbol{U}^*, \quad \boldsymbol{r} = R_0 \boldsymbol{r}^*, \quad t = (R_0/U_0)\, t^*, \quad P = \varrho_0 U_0^2 P^* \tag{8}$$

into (1), (5), (6) and (7). The values of $U_0$, $R_0$ and so forth need not be identical with those given in Table 1 as that table only gives orders of magnitude. Generally $U_0$ is the centerline velocity of the Hagen-Poiseuille flow, $R_0$ the pipe radius and $\varrho_0$ the density of the fluid. At places where electromagnetic fields are involved we put

$$\boldsymbol{E} = E_0 \boldsymbol{E}^* \quad \text{and} \quad \boldsymbol{B} = B_0 \boldsymbol{B}^* \tag{9}$$

and agree upon choosing for $E_0$ and $B_0$ the absolutely largest values of the electric and magnetic fields within the pipe. Because of (5) and (6) we are sure to find the maxima on the pipe wall.

All this makes from (1) and (5)–(7)

$$\frac{\mathrm{d}\boldsymbol{U}^*}{\mathrm{d}t^*} = -\nabla^* P^* - \frac{1}{Re} \nabla^* \times \nabla^* \times \boldsymbol{U}^* + \frac{1}{Ma^2} \boldsymbol{E}^* \times \boldsymbol{B}^* \quad \text{with} \quad \nabla^* \cdot \boldsymbol{U}^* = 0 \tag{10}$$

and

$$\nabla^* \times \boldsymbol{B}^* = 0, \quad \nabla^* \cdot \boldsymbol{B}^* = 0, \tag{11}$$

$$\nabla^* \times \boldsymbol{E}^* = 0, \quad \nabla^* \cdot \boldsymbol{E}^* = 0. \tag{12}$$

From here on, the asterisks are omitted, but it is understood that all forthcoming equations are written in terms of nondimensional units.

Equation (10) contains two characteristic quantities. The Reynolds number

$$Re := \frac{U_0 R_0}{\nu_0} \tag{13}$$

measures the dominance of inertia over viscosity. Reynolds numbers at 2000 are customary in studies of transition to turbulence. We call

$$Ma := \sqrt{\frac{\varrho_0 \nu_0^2 Re^2}{\sigma_0 E_0 B_0 R_0^3}} \tag{14}$$

the Mach-Alfvén number. It compares the importance of inertia with magnetic deflection. With the values in Table 1 we find $Ma \approx 0.3$. This should be small enough for noticeable magnetohydrodynamic effects.

The differential equations must be completed by initial and boundary conditions. They will be given when (10)–(12) are actually solved, i.e. in the next two sections.

## 3. Two Classes of Magnetic Fields

Now (11) and (12) will be solved in cylindrical coordinates $r$, $\varphi$, $z$, with unit vectors $\boldsymbol{e}_r$, $\boldsymbol{e}_\varphi$, $\boldsymbol{e}_z$. Let the origin of the coordinate system lie in the middle of the pipe, in particular where the test section begins; $\boldsymbol{e}_z$ should point in the direction of the pipe's axis.

Equations (12) can be solved without calculation. There are electrodes at inlet and outlet of the pipe. Therefore the electric field is homogeneous in the test section,

$$\boldsymbol{E}(r, t) = \boldsymbol{e}_z E_0 \{\Theta(t) - \Theta(t-T)\} . \tag{15}$$

$\Theta(t)$ denotes Heaviside's function, i.e. the electric field is switched on at $t=0$ and off at $t=T$.

The Lorentz term in (10) indicates that it is enough to vary the electric field. We can afford a constant magnetic field. This is comfortable since switching big magnets can cause trouble.

The equations in (11) constitute a common problem of potential theory. They can be solved via potentials [10, 11]

$$\boldsymbol{B} = \boldsymbol{B}^{|} + \boldsymbol{B}^{+} \quad \text{with} \quad \boldsymbol{B}^{|} := \nabla \times \boldsymbol{e}_z a \quad \text{and} \quad \boldsymbol{B}^{+} := \nabla c , \tag{16}$$

where the scalar functions $a$ and $c$ both satisfy Laplace's equation.

From the construction in (16) it follows that $\boldsymbol{B}^{|}$ has no component along $\boldsymbol{e}_z$. Therefore it is flat and everywhere perpendicular to the basic fluid flow. $\boldsymbol{B}^{+}$, in contrast, may have a $z$-component. I want to stress this difference because only $\boldsymbol{B}^{+}$ will turn out to be a good exciter of turbulence. Although it is hard in practice to generate a magnetic field without component parallel to the flow, it should be feasible to vary the size of the parallel component without reducing the absolute strength of the field. Already this would allow to check the theory of turbulence generation in a pipe.

For the two potentials in (16) we may take

$$a = \begin{cases} -N_0^{-1} J_0(\gamma r) & \text{if} \quad m=0 \\ -N_0^{-1} J_m(\gamma r) \sin m\varphi \cdot e^{-\gamma z} & \text{otherwise,} \end{cases} \tag{17}$$

$$c = -N_0^{-1} J_m(\gamma r) \cos m\varphi \cdot e^{-\gamma z} \tag{18}$$

with Bessel functions of integer order $J_m$ [12]. Thus $a$ and $c$ fulfil Laplace's equation. $N_0$ is a normalization factor. These functions model stray fields behind the shoes of a magnet with multipolarity $m \geq 0$. Notice the factor $e^{-\gamma z}$: $1/\gamma$ measures the extension of the magnetic field. Hence we demand $\gamma > 0$.

Between the shoes, (17), (18) give no good description. However, in the next section we will see that it is only the change $\partial \boldsymbol{B}/\partial z$ which deflects the flow, rather than the absolute value of the magnetic field $\boldsymbol{B}$. Therefore we need an appropriate representation of the stray fields. Another way to say the same is that (17) and (18) incorporate the boundary condition on $\boldsymbol{B}$ for $z \to \infty$.

Evaluation of (17) and (18) by (16) produces

$$\boldsymbol{B}^{|} = \boldsymbol{e}_r \frac{-1}{N_0} \frac{m}{r} J_m(\gamma r) \cos m\varphi \cdot e^{-\gamma z} + \boldsymbol{e}_\varphi \frac{1}{N_0} \gamma J_m'(\gamma r) \sin m\varphi \cdot e^{-\gamma z} \tag{19}$$

with $N_0 = \max(|\gamma J_m'(\gamma)|, |m J_m(\gamma)|, |\xi|)$ and

$$\boldsymbol{B}^{+} = \boldsymbol{e}_r \frac{-1}{N_0} \gamma J_m'(\gamma r) \cos m\varphi \cdot e^{-\gamma z} + \boldsymbol{e}_\varphi \frac{1}{2N_0} \frac{m}{r} J_m(\gamma r) \sin m\varphi \cdot e^{-\gamma z} + \boldsymbol{e}_z \frac{1}{2N_0} \gamma J_m(\gamma r) \cos m\varphi \cdot e^{-\gamma z} \tag{20}$$

with $N_0 = \max(|\gamma| \sqrt{J_m^2(\gamma) + J_m'^2(\gamma)}|, |m J_m(\gamma)|, |\xi|)$. In (19), $\xi$ takes the values $\gamma/2$ or 0 depending on $m$ being

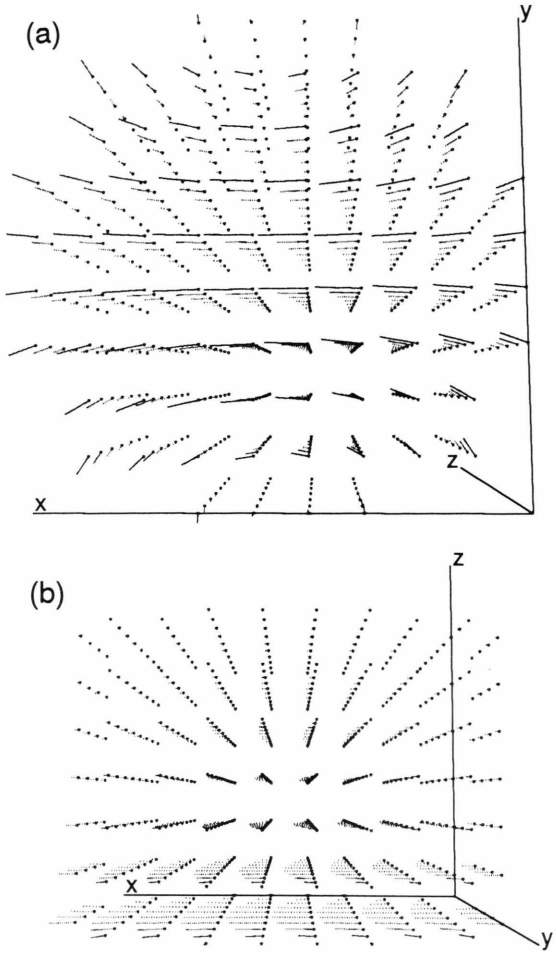


Fig. 1. Two views of the magnetic field $\boldsymbol{B}^{|}$ for azimuthal node number $m=1$ and range-of-force parameter $\gamma=2$ according to (19). Both views show only those vectors that fit into a pipe. Part (a) displays the perspective one has when one looks into the pipe from its inlet; the axis $z$ is parallel to the centerline of the pipe. Part (b) presents the corresponding side-perspective. To obtain Part (b) from Part (a), clutch the $y$-axis in Part (a) and draw it letting the figure rotate about the $x$-axis. Lengths are such that $x$ and $y$ vary from $-1$ to $+1$, and $z$ increases from 0 to 2. All vectors are drawn as hatched lines. The hatching becomes thinner for vectors in the farther background. The points of attachment appear as dots. Three items should be noticed: Firstly the decrease of the field with $z$. Secondly the perfect flatness of $\boldsymbol{B}^{|}$; it has no component in the $z$-direction and hence no component in the direction of the basic flow: see Part (b). Thirdly the concave structure as apparent in Part (a). If flatness is desired, concavity is unavoidable due to the nondivergence of the magnetic field. This observation gives clues concerning the generation of flat fields: Magnetic shoes are needed that embrace the pipe.

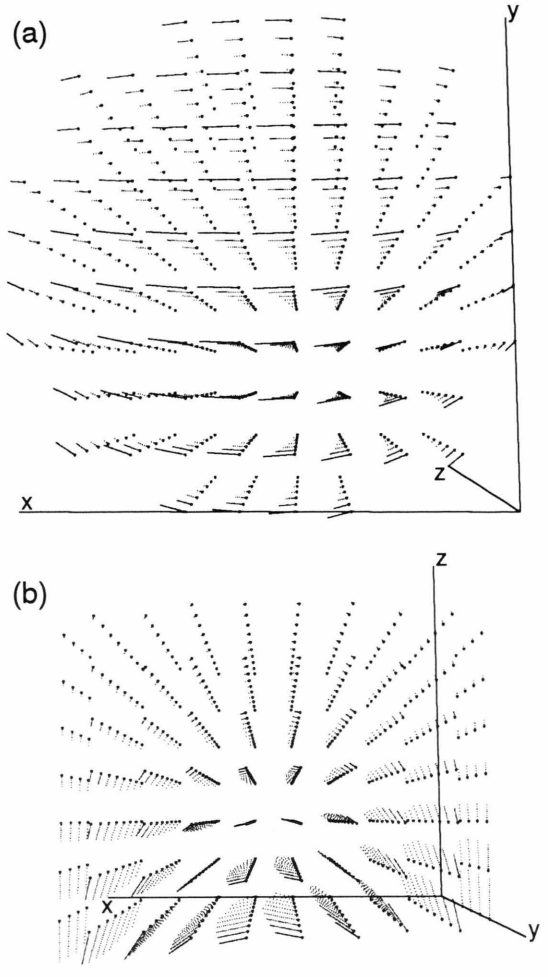


Fig. 2. Two views of the magnetic field $\boldsymbol{B}^{+}$ for azimuthal node number $m=1$ and range-of-force parameter $\gamma=2$ according to (20). Otherwise this figure is similar to Figure 1. In Part (b) it should be noticed, however, that this field has considerable $z$-components, i.e. components parallel to the basic flow. Consequently it is convex, see Part (a). It takes a magnet with tapering shoes to create a field like this. – Figures 1 and 2 were made using the software RELATION.

1 or something else. For (20), $\xi$ is the same except that it must be $\gamma$ for $m=0$. The normalization factors $N_0$ are such that moduli of the magnetic fields never exceed 1 for $r\leq 1$ and $z\geq 0$. For the sake of realism $\gamma$ should be small enough to keep $J'_m(\gamma)$ above zero.

Fields of the type (19) and (20) are displayed in Figs. 1 and 2.

## 4. The Equations of Motion

For incompressible fluids, the vorticity equation is a more convenient description of motion than the Navier-Stokes equation (10). However, the first is easily obtained from the latter by taking the curl. Let us concentrate first on the Lorentz term

$$\nabla\times(\boldsymbol{E}\times\boldsymbol{B})=\boldsymbol{E}\,\nabla\cdot\boldsymbol{B}-\boldsymbol{B}\,\nabla\cdot\boldsymbol{E}+\boldsymbol{B}\cdot\nabla\boldsymbol{E}-\boldsymbol{E}\cdot\nabla\boldsymbol{B}\,. \quad (21)$$

The first two terms on the right-hand side disappear due to the divergence-zero equations in (11) and (12). The third term gives nothing since according to (15) $\boldsymbol{E}$ is constant in space. Equation (15) also serves to simplify the fourth term so that the vorticity equation reads

$$\frac{\partial\boldsymbol{W}}{\partial t}=\nabla\times(\boldsymbol{U}\times\boldsymbol{W})-\frac{1}{Re}\nabla\times\nabla\times\boldsymbol{W}-\frac{1}{Ma^2}\frac{\partial\boldsymbol{B}}{\partial z}\,, \quad (22)$$

where

$$\boldsymbol{W}:=\nabla\times\boldsymbol{U} \quad (23)$$

denotes the vorticity. Equation (22) proves the announcement made in the previous chapter: Only spatial variations of the magnetic field $\boldsymbol{B}$ modify the fluid motion.

The argument depends on the equivalence of the vorticity description with the velocity representation. The equivalence, however, becomes questionable if free boundary conditions are involved [7]. Fortunately, this is not the case here.

Equation (22) is solved by means, the details of which are given elsewhere [5]. We outline here only fundamentals. The solution is expanded as

$$\boldsymbol{U}(\boldsymbol{r},t)=\boldsymbol{e}_z(1-r^2)+\sum_\nu a_\nu(t)\,\boldsymbol{s}_\nu(\boldsymbol{r})\,. \quad (24)$$

The term with $1-r^2$ describes the well-known Hagen-Poiseuille profile which represents the basic flow. The symbols $\boldsymbol{s}_\nu(\boldsymbol{r})$ denote Stokes functions that satisfy the linearized Navier-Stokes equations for small Reynolds numbers; they and their vorticities constitute orthogonal systems; they have zero divergence and describe non-slip behaviour along the walls of the pipe. Hence incompressibility

$$\nabla\cdot\boldsymbol{U}(\boldsymbol{r},t)=0 \quad (25)$$

and the boundary condition

$$\boldsymbol{U}(r=1,\varphi,z,t)=\boldsymbol{0} \quad (26)$$

of the solution $\boldsymbol{U}$ are warranted.

One inserts (24) and the corresponding series for $\boldsymbol{W}$ in (22), multiplies this equation by the complex conjugate $\boldsymbol{w}^*_\lambda(\boldsymbol{r}):=\nabla\times\boldsymbol{s}^*_\lambda(\boldsymbol{r})$ and integrates it over the relevant piece of the pipe. In this way a system of ordinary differential equations

$$\frac{\mathrm{d}a_\lambda(t)}{\mathrm{d}t}=W^{\mu\nu}_\lambda\,a_\mu(t)\,a_\nu(t)+H^\mu_\lambda\,a_\mu(t)-\frac{\alpha^2_\lambda}{Re}a_\lambda(t)-\frac{1}{Ma^2}f_\lambda(t) \quad (27)$$

is obtained. Summations are done according to Einstein's convention. The interaction matrix $W^{\mu\nu}_\lambda$, the Hagen matrix $H^\mu_\lambda$ and the damping terms $\alpha^2_\lambda/Re$ are exactly the same as in [5]. New is the driving force

$$f_\lambda(t):=\frac{1}{\alpha^2_\lambda}\int_{(\mathrm{pipe})}\boldsymbol{w}^*_\lambda(\boldsymbol{r})\frac{\partial\boldsymbol{B}(\boldsymbol{r})}{\partial z}\,\mathrm{d}\tau\cdot\{\Theta(t)-\Theta(t-T)\}\,. \quad (28)$$

We compute all integrals using known methods and solve the differential equations (27) numerically [5].

Here, in contrast to [5], only solutions of the linearized equations (27) will be presented. Only the startup shall be studied where all amplitudes $a_\lambda(t)$ are still small. Linearization amounts to putting $W^{\mu\nu}_\lambda=0$. In this case the system (27) separates. That is, the $\lambda$, $\mu$ or $\nu$ are compounds consisting of three numbers: $\nu=(n,m,\beta)$. $n$ counts the nodes of the respective Stokes function in radial direction, $m$ gives the azimuthal nodes, and $\beta$ is the longitudinal wavenumber of the disturbance. Separation means that only Stokes modes with different $n$'s are coupled. It is possible to fix $m$ and $\beta$. For all solutions of (27), Stokes modes with $n=1,2,\ldots,20$ were included and the results analyzed for $m=0$, 1, 2 or 3. Likewise systematics were created for $\beta=0.25$, 0.5, 1.0 or 2.0.

## 4. Predictions

With some knowledge on the mechanism of energy transfer from the basic flow to the disturbances, all results turned out to be immediately intelligible. Let us recall here the essentials of that mechanism: Energy transfer in pipe flow is possible because all disturbances are divided in two classes of flows, mothers and daughters [5]. Only the mothers can draw energy from the basic flow. However, they don't keep it but pass it to their daughters. Controlling turbulence hence amounts to rule the mothers. Mothers and daughters are geometrically different: Mothers cannot be axially

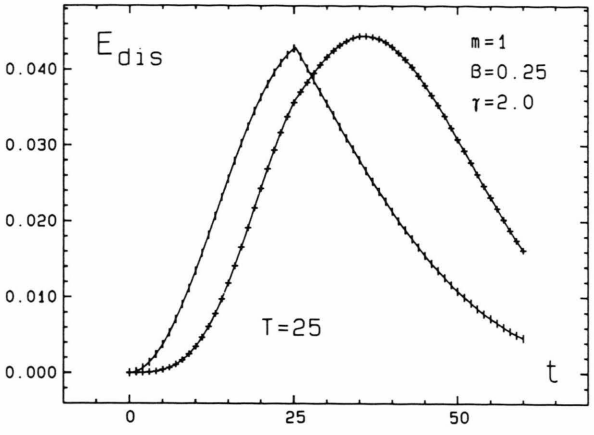


Fig. 3. The energy of the disturbance $E_{\text{dis}}$ varying with time $t$. The two curves are results of trajectory calculations based on the equations of motion (27) with the forces $f_\lambda(t)$ given by (28). The magnetic force was switched off at $T=25$. The curve, distinguished by the | symbols, displays what came out when the flat magnetic field $\boldsymbol{B}^{|}$ ((19), Fig. 1) was applied. The curve with the +'s was obtained using the curved magnetic field $\boldsymbol{B}^{+}$ ((20), Fig. 2). For the +'s it is seen that the excitation continues to grow for some time even when the magnetic force was switched off. In the case with the |'s, the excitation drops directly after the removal of the electromagnetic interaction.

symmetrical ($m \neq 0$), and they have almost no component in the direction of the Hagen-Poiseuille flow.

Now here is a list of the results:

(i) The difference between the induction of a mother-daughter cycle and a daughterly excitation shows up at its best in the lifetime of the disturbance: The mother-daughter cycle reaches its maximum long after the electromagnetic interaction was switched off, while pure daughters die away as soon as the impellent disappears.

(ii) Only magnetic fields with a strong component along the pipe's axis, $\boldsymbol{B}^{+}$ according to (16) and (20), induce a mother-daughter cycle.

(iii) The magnetic field should have a range as short as possible. More precisely, $1/\gamma \approx 0.5\, R_0$ is desired.

(iv) The multipolarity of the magnetic field should be $m=1$.

(v) The duration of the electromagnetic pulse should be $T \approx 20\, R_0/U_0$.

(vi) The differences between a mother-daughter cycle and decaying daughters can be seen most clearly in the long-wave disturbances: One should observe wavelengths as long as $2\pi/\beta = 8\pi R_0$.

Figure 3 is an illustration of item (i). It shows the evolution of two disturbances measured by their energies

$$E_{\text{dis}}(t) = \tfrac{1}{2} \sum_{\nu} |a_\nu(t)|^2 . \tag{29}$$

There is no disturbance at $t=0$,

$$\boldsymbol{U}(\boldsymbol{r}, t=0) = \boldsymbol{e}_z(1-r^2) \quad \text{or equivalently}$$

$$a_\lambda(t=0) = 0 \quad \text{for all } \lambda, \tag{30}$$

and the electromagnetic force is switched on only at $t=0$. Then the disturbance increases, induced either by the flat field $\boldsymbol{B}^{|}$ as described by (19) or by the curved one $\boldsymbol{B}^{+}$ given in (20). The corresponding curves in Fig. 3 are marked by |'s and +'s. At $T=25$ the force is switched off. The force with the flat field causes an excitation, but when this force is gone, its excitation fades as well. The curved field is first much less effective. Nevertheless, its excitation *continues to grow* even when the force is cancelled.

This behaviour is based on the most fundamental property of a mother, namely that no mother can make a big flurry. It's only their daughters which become strong enough. Here it matters much to consider the sequence in time: Mothers decay, but while they decay, they give rise to daughters being much more powerful. The daughters, however, just fade [5]. Hence we could understand Fig. 3 if we knew why flat fields induce only daughters whereas curved fields have access to mothers.

To explain this, remember that mothers have almost no common component with the basic flow (compare Fig. 26 in [5]). As a consequence, motherly vorticities are unidirectional fields: $\boldsymbol{W} \propto \boldsymbol{e}_z$. If a magnetic field $\boldsymbol{B}$ is to induce a certain vorticity, it must be, according to (22), at least partially parallel to $\boldsymbol{W}$. From a look on Figs. 1 and 2 we understand that only curved fields $\boldsymbol{B}^{+}$ are suitable. The flat fields $\boldsymbol{B}^{|}$ have no $z$-component and induce thus only daughters. Item (ii) summarizes this result.

To substantiate item (iii) consider Table 2. Obviously the fields with the biggest $\gamma$, i.e. with the shortest range, generate the greatest disturbances. The fact is immediately understandable from (22) as only $\partial \boldsymbol{B}/\partial z$ enters that equation, and our $\partial \boldsymbol{B}/\partial z$'s are all proportional to $\gamma$, see (19) and (20). $\gamma$'s greater than 2 do not seem to be practical: Fig. 2b exhibits that the force lines are almost parallel to the pipe wall. This can be achieved only when the magnetic shoes are pressed to the tube. Further approach would crush it.

Numbers to support item (iv) are presented in Table 3. Clearly with $m=1$ the greatest disturbances

Table 2. The size of the excitation as a function of the range-of-force parameter $\gamma$. The times $t_{max}$, for which the excitation reaches its maximum, and the corresponding energy $E_{dis}(t_{max})$ of the disturbance are reported. The right-hand side presents these quantities for the force without component parallel to the basic flow (symbol |). On the left-hand-side one can find the same information for the force with parallel component (symbol +). The duration of the electromagnetic interaction was always $T=25$, and the geometrical parameters were $m=1$ and $\beta=0.25$. Thus the results given in the last line were produced by the magnetic fields displayed in Figs. 1 and 2.

| $t^+_{max}$ | $E^+_{dis}(t_{max})$ | $\gamma$ | $t^\perp_{max}$ | $E^\perp_{dis}(t_{max})$ |
|---|---|---|---|---|
| 25 | 0.0001 | 0.5 | 25 | 0.0003 |
| 33 | 0.0016 | 1.0 | 25 | 0.0043 |
| 36 | 0.0107 | 1.5 | 25 | 0.0173 |
| 36 | 0.0446 | 2.0 | 25 | 0.0428 |

Table 3. The size of the excitation as a function of the azimuthal node number $m$. The structure of this table is similar to Table 2. Notice that here the duration $T$ of the electromagnetic interaction was varied to produce the biggest excitation possible. In all cases, the geometrical parameters were $\beta=0.25$ and $\gamma=2.0$.

| $T^+$ | $t^+_{max}$ | $E^+_{dis}(t_{max})$ | $m$ | $T^\perp$ | $t^\perp_{max}$ | $E^\perp_{dis}(t_{max})$ |
|---|---|---|---|---|---|---|
| 20 | 20 | 0.0055 | 0 | 21 | 21 | 0.0007 |
| 22 | 35 | 0.0446 | 1 | 29 | 29 | 0.0441 |
| 24 | 36 | 0.0066 | 2 | 30 | 30 | 0.0046 |
| 26 | 37 | 0.0008 | 3 | 31 | 31 | 0.0005 |

Table 4. The size of the excitation as a function of the longitudinal node number $\beta$: The wavelength of the excitation produced is $2\pi R_0/\beta$, where $R_0$ denotes the pipe's radius. This table is constructed as Tables 2 and 3. Please see the remarkable variation of the optimum duration $T$ with $\beta$.

| $T^+$ | $t^+_{max}$ | $E^+_{dis}(t_{max})$ | $\beta$ | $T^\perp$ | $t^\perp_{max}$ | $E^\perp_{dis}(t_{max})$ |
|---|---|---|---|---|---|---|
| 22 | 35 | 0.045 | 0.25 | 29 | 29 | 0.044 |
| 16 | 16 | 0.020 | 0.50 | 14 | 14 | 0.049 |
| 7.5 | 7.5 | 0.015 | 1.00 | 7.1 | 7.1 | 0.051 |
| 3.1 | 3.1 | 0.013 | 2.00 | 3.1 | 3.1 | 0.036 |

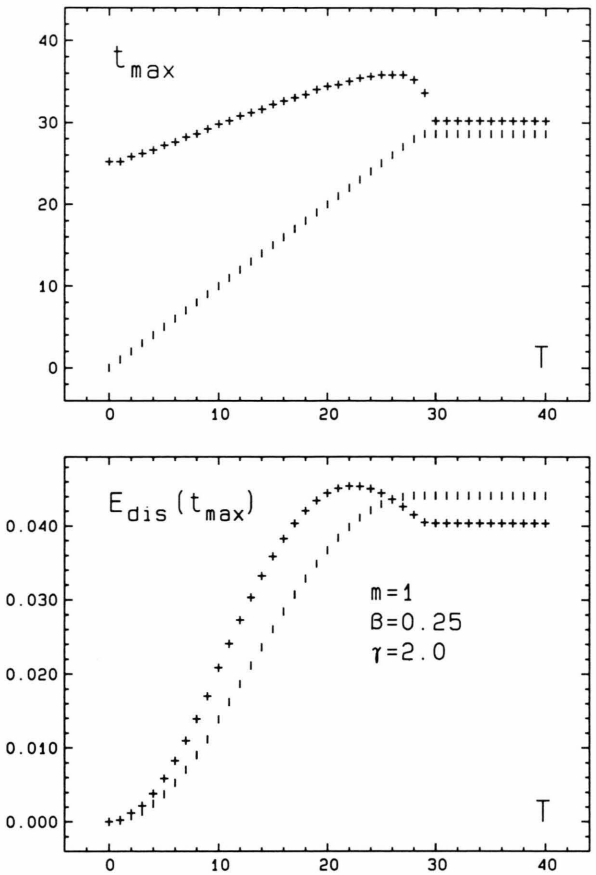


Fig. 4. Maximal excitation as a function of the duration $T$ of the electromagnetic interaction. In the upper part, the time $t_{max}$ is given at which the maximum of $E_{dis}(t)$ is reached. The lower part reproduces the actual values of $E_{dis}(t_{max})$. For the case wih the flat magnetic field, marked off by | symbols, we find $t_{max}=T$ until saturation is reached. By contrast, the curved magnetic field (+ symbols) allows $t_{max}>T$ if $T$ isn't to big. This is the same information as conveyed by Fig. 3, namely the continued growth. Here we see the systematic variation of the effect with $T$. The saturation is related to the eigenvalues of the force-free, time-separated problem. At $\beta=0.25$ these eigenvalues are such that for times greater than 30 damping and dephasing overthrow the growth induced by the magnetic forces.

are created. For $m>1$ mothers exist, but their excitation is not sufficiently effective. The predominance of $m=1$ is comfortable for the practitioner as it is easiest to construct magnets close to bipolarity. By the way, Table 3 confirms the known fact that axially symmetrical mothers do not exist [5]. In this case continued growth does not occur; $T^+$ and $t^+_{max}$ coincide for $m=0$.

From Fig. 3 one can read the time $t_{max}$ at which the excitation gets maximum, and one may read the respective energy $E_{dis}(t_{max})$ for a definite duration $T$ of the interaction. Moreover one can optimize $T$ such that $E_{dis}(t_{max})$ becomes as large as possible. Figure 4 may be used for this purpose: From the lower part we find that $E^+_{dis}(t_{max})$ is greatest for $T^+=22$. The corresponding time can be taken from the upper part: $t^+_{max}=35$. Exactly these numbers may be rediscovered in the Tables 3 and 4.

Although it is desirable to have effects as large as possible, one also wants to detect if a mother or only daughters were excited. The best criterion is the *con-*

*tinued growth* which is expressed in the upper part of Fig. 4 by the excess of +'s over the |'s. The excess is biggest close to $T=0$, but with these short durations the excitations cannot become strong. Hence $T \approx 20$ is a reasonable compromise, compare item (v) above.

Table 4 looks much the same as Table 3. In fact, it presents the size of the maximal disturbance depending on $\beta$. The difference to the previous tables is that $\beta$ is not predetermined by the experiment. $\gamma$ and $m$ are fixed by the shape of the external magnet. The real disturbances come, however, as superpositions of elementary disturbances with all possible $\beta$'s. Table 4 communicates that one should look for the long-wave disturbances as they are produced with greatest effectiveness. Moreover, the discrimination between mothers and daughter is more difficult at larger $\beta$'s. Compare item (vi). Nevertheless, it does not seem sensible to look for too long wavelengths since only disturbances with $\beta$'s not substantially lower 1 can contribute to turbulence [5].

## 5. Application to a Real Experiment

All calculations were performed with a Mach-Alfvén number $Ma=0.3$. This value is suggested by the numbers presented in Table 1. The effects are powerful enough: One reads from Figs. 3 and 4 and from the Tables 2 thru 4 that $E_{\mathrm{dis}}(t_{\max}) \approx 0.04$ can be reached. This is much since the energy of the Hagen-Poiseuille basic flow per length unit is not more than $1/12 \approx 0.08$.

The equation of motion (27) is linear. Amplitudes vary with $Ma^{-2}$ and energies hence with $Ma^{-4}$. Knowing the results for one value of the Mach-Alfvén number is therefore sufficient.

The Kiel experiment [6, 8] works with water and the following parameters: $Re=2000$, $E_0=167\ \mathrm{V\,m^{-1}}$, $J_0=\sigma_0 E_0=2300\ \mathrm{A\,m^{-2}}$, $B_0=0.4\ \mathrm{V\,m^{-2}\,s}$ and $R_0=6.5\cdot 10^{-3}\ \mathrm{m}$. Inserting this into (14) gives $Ma=4$. This value is much too high. In fact, the experimenters observe effects, but they are so small that they can just be seen. To improve on this, it might be worthwhile to realize that $R_0$ enters $1/Ma^2$ with the third power.

[1] W. Tollmien, Nachr. Ges. Wiss. Göttingen, Math. Phys. Klasse (1929), p. 21, H. Schlichting, Grenzschicht-Theorie, 8. Auflage, Braun, Karlsruhe 1982, Kap. XVI.
[2] G. B. Schubauer and H. K. Skramstad, J. Aeronaut. Sci. **14,** 69 (1947).
[3] G. Redeker, Flugversuche zum Laminarflügel, VDI nachrichten magazin 2/88 (1988).
[4] R. J. Leite, J. Fluid Mech. **5,** 81 (1959).
[5] L. Boberg and U. Brosa, Z. Naturforsch. **43a,** 697 (1988).
[6] F. Obermeier, T. Reimers, E. O. Schulz-DuBois, B. Staabs, and V. Wilkening, Visualization Studies of the Onset of Turbulence in Pipe Flow. Contribution to the 4th International Conference on Laser Anemonetry, Cleveland, Ohio 1991.
[7] G. E. A. Meier, private communication.
[8] E. O. Schulz-DuBois, G. E. A. Meier, and U. Brosa, Application to the Volkswagen Foundation, Approved Project I/65331 (1989).
[9] J. D. Jackson, Classical Electrodynamics, 2nd edition, Wiley, New York 1975, Chapt. 10.
[10] S. Großmann, Mathematischer Einführungskurs für die Physik, 5. Auflage, Teubner, Stuttgart 1988, Kap. 8.6.
[11] U. Brosa, Zur Lösung von Randwertproblemen mit Vektorfeldern, Habilitationsschrift, Philipps Universität, Marburg 1985.
[12] M. Abramowitz and I. A. Stegun (editors), Handbook of Mathematical Functions, Dover, New York 1972, Chapt. 9.